

Ground state of electron-doped t–t'–J model on cylinders: An investigation of finite size and boundary condition effects

Yang Shen(沈阳), Xiangjian Qian(钱湘坚), and Mingpu Qin(秦明普)
Citation: Chin. Phys. B, 2025, 34 (**8**): 087105. DOI: 10.1088/1674-1056/add00b
http://cpb.iphy.ac.cn; http://iopscience.iop.org/cpb

What follows is a list of articles you may be interested in

Momentum-dependent anisotropy of the charge density wave gap in quasi-1D $ZrTe_{3-x}Se_x$ (x = 0.015)

Renjie Zhang(张任杰), Yudong Hu(胡裕栋), Yiwei Cheng(程以伟), Yigui Zhong(钟益桂), Xuezhi Chen(陈学智), Junqin Li(李俊琴), Kozo Okazaki, Yaobo Huang(黄耀波), Tian Shang(商恬), Shifeng Jin(金士锋), Baiqing Lv(吕佰晴), and Hong Ding(丁洪)
Chin. Phys. B, 2025, 34 (**7**): 077106. DOI: 10.1088/1674-1056/addcc5

Competing phases and suppression of superconductivity in hole-doped Hubbard model on honeycomb lattice

Hao Zhang(张浩), Shaojun Dong(董少钧), and Lixin He(何力新)
Chin. Phys. B, 2025, 34 (**7**): 077102. DOI: 10.1088/1674-1056/adcb20

Electronic structure and disorder effect of $La_3Ni_2O_7$ superconductor

Yuxin Wang(王郁欣), Yi Zhang(张燚), and Kun Jiang(蒋坤)
Chin. Phys. B, 2025, 34 (**4**): 047105. DOI: 10.1088/1674-1056/adbacc

Electronic structure from equivalent differential equations of Hartree-Fock equations

Hai Lin(林海)
Chin. Phys. B, 2019, 28 (**8**): 087101. DOI: 10.1088/1674-1056/28/8/087101

Phase diagram of the Fermi–Hubbard model with spin-dependent external potentials: A DMRG study

Wei Xing-Bo (魏兴波), Meng Ye-Ming (孟烨铭), Wu Zhe-Ming (吴哲明), Gao Xian-Long (高先龙)
Chin. Phys. B, 2015, 24 (**11**): 117101. DOI: 10.1088/1674-1056/24/11/117101

Ground state of electron-doped t–t'–J model on cylinders: An investigation of finite size and boundary condition effects

Yang Shen(沈阳)[1], Xiangjian Qian(钱湘坚)[1], and Mingpu Qin(秦明普)[1,2,†]

[1] *Key Laboratory of Artificial Structures and Quantum Control (Ministry of Education), School of Physics and Astronomy, Shanghai Jiao Tong University, Shanghai* 200240, *China*
[2] *Hefei National Laboratory, Hefei* 230088, *China*

(Received 20 February 2025; revised manuscript received 22 April 2025; accepted manuscript online 24 April 2025)

We perform a comprehensive study of the electron-doped t–t'–J model on cylinders with density matrix renormalization group (DMRG). We conduct a systematic study on the finite-size and boundary condition effects on t–t'–J model on cylinders. Periodic and anti-periodic boundary conditions are implemented along the circumference direction, with the system's width extending up to as large as 8 lattice units. We study doping levels of $1/6$, $1/8$, and $1/12$, which represent the most interesting region in the phase diagram of electron-doped cuprates. We find that for width-4 and width-6 systems, the ground state for fixed doping switches between anti-ferromagnetic Neel state and stripe state under different boundary conditions and system widths, indicating the presence of large finite size effect in the t–t'–J model. We also have a careful analysis of the d-wave pairing correlations which also change quantitatively with boundary conditions and widths of the system. However, the pairing correlations are enhanced when the system becomes wider for all dopings, suggesting the existence of possible long-range superconducting order in the thermodynamic limit. The width-8 results are found to be dependent on the starting state in the DMRG calculation for the kept states we can reach. For the width-8 system, only Neel (stripe) state can be stabilized in DMRG calculation for $1/12$ ($1/6$) doping, while both stripe and Neel states are stable in the DMRG sweep for $1/8$ doping, regardless of the boundary conditions. These results indicate that $1/8$ doping is likely to lie on the boundary of a phase transition between the Neel phase with lower doping and the stripe phase with higher doping, consistent with the previous study. The sensitivity of the ground state on boundary conditions and size observed for narrow systems is similar to that found in the t'-Hubbard model, where the t' term introduces frustration and makes the stripe state fragile. The study of different boundary conditions provides a useful tool to check the finite size effect in the future DMRG calculations.

Keywords: t–t'–J model, finite-size effect, boundary conditions, DMRG, superconductivity

PACS: 71.10.Fd, 74.72.–h, 64.60.an, 05.10.Cc

DOI: 10.1088/1674-1056/add00b **CSTR:** 32038.14.CPB.add00b

1. Introduction

Hubbard model and its descendant t–J model[1–8] play a paradigmatic role in the study of strongly correlated quantum many-body physics.[9,10] Though their forms are simple, many exotic quantum states are arguably related to these models. It is believed that these models on square lattice are connected to the high-T_c superconductivity in cuprates.[2,9–12] Recent state-of-the-art numerical results show that the ground state of pure Hubbard model (with only nearest hoppings) is a stripe state[13,14] without long-range superconductivity,[15] which indicates the necessity to modify the Hamiltonian if we want to pursue superconducting ground state in the single-band framework.

It is well known that the next nearest neighboring hopping t' term is necessary to account for the particle–hole asymmetry in the phase diagram of cuprates.[9] Band structure calculations[16,17] also show the existence of a $t' \approx -0.2$ term in the single band description of cuprates. The effect of the t' term on the ground state of Hubbard and t–J models was extensively explored before.[18–39] The t' term frustrates and weakens the long-range antiferromagnetic Neel order in the parent compound. When the system is doped, the stripe order should also be suppressed by the t' term which is believed to benefit superconducting pairing. Calculations on the t–t'–J model[25–27] show the ground state turns into a superconducting one in the electron doped side. Superconductivity was also found in the t'-Hubbard model[40] and matches quantitatively with the phase diagram of cuprates, in which superconductivity is stronger in the hole doped side than that in the electron doped side.

One of the important findings in Ref. [40] is that the ground state of the t'-Hubbard model becomes very sensitive to the system width and boundary conditions, which indicates the presence of large finite size effect in the model. For this reason, the authors in Ref. [40] utilized twist averaged boundary conditions and careful finite size scaling to obtain physical quantity in the thermodynamic limit. For the t–t'–J model, the most recent studies[27,29] on cylinders with finite width show that the superconductivity is stronger in the electron doped

†Corresponding author. E-mail: qinmingpu@sjtu.edu.cn

© 2025 Chinese Physical Society and IOP Publishing Ltd. All rights, including for text and data mining, AI training, and similar technologies, are reserved.

side than that in the hole doped side if it exists, contradictory to the phase diagram of cuprates and the recent results of the t'-Hubbard model.[40] Given the presence of very large finite size effect in the t'-Hubbard model, it is natural to ask whether the t–t'–J model also has large finite size effect and how it influences the superconducting behaviors, which will be ultimately beneficial to resolve the inconsistency between the t'-Hubbard and the t–t'–J models.

While previous study[23] with only periodic boundary condition also indicates finite-size effect on hole doped t'-Hubbard model by observing the change of pairing symmetry for different system widths, exploring the sensitivity of boundary conditions is another useful and complementary indicator to reflect properties in the two-dimensional thermodynamic limit, especially when DMRG calculations on wider (> 8) cylinder systems are not accessible at present. In this work, we conduct a comprehensive study of the t–t'–J model with density matrix renormalization group (DMRG)[41–43] by adopting both periodic and anti-periodic boundary conditions along the circumference direction, in conjunction with different system widths, to explore its finite size effect.[40] We only study the electron doped side in this work, which was believed to be simpler than the hole doped side, without the competition of different states.[9] We study doping levels of $1/6$, $1/8$, and $1/12$ which represent the most interesting region in the phase diagram of electron-doped cuprates.

Our results show that the ground state of the t–t'–J model is also very sensitive to the boundary conditions and width of the systems, similar to the t'-Hubbard model.[40] We find that for width-4 and width-6 systems, the ground state for fixed doping switches between anti-ferromagnetic Neel state and stripe state under different boundary conditions and with system widths. We find the pairing correlation also changes quantitatively with boundary conditions and widths. But for all dopings, the pairing correlations are enhanced when the system becomes wider, suggesting the existence of possible long-range superconducting pairing in the thermodynamic limit. The width-8 results are found to be dependent on the starting state in the DMRG calculation for the kept states we can reach. For the width-8 system only Neel (stripe) state can be stabilized in DMRG calculation for $1/12$ ($1/6$) doping, while both stripe and Neel states are stable in the DMRG sweep for $1/8$ doping. Although a reliable finite width scaling of the DMRG results is infeasible at present, these results indicate that $1/8$ doping is likely to lie on the boundary of the phase transition between the Neel state with lower doping and stripe state with higher doping, consistent with the previous study.[27]

The rest of this paper is organized as follows. In Section 2, we discuss the t–t'–J model and the detailed method we employ. Our results under various boundary conditions and within different size constraints are presented in Section 3 starting with the spin and charge densities, followed by an analysis of the pairing correlations. In Section 4, we have a discussion of the intricate relationship between superconductivity and stripe based on the above results. We finally conclude this work in Section 5.

2. Model and methods

The Hamiltonian for the t–t'–J model is defined as

$$H = -t \sum_{\langle i,j\rangle,s} c^{\dagger}_{i,s} c_{j,s} - t' \sum_{\langle\langle i,j\rangle\rangle,s} c^{\dagger}_{i,s} c_{j,s} + J \sum_{\langle i,j\rangle} S_i S_j, \qquad (1)$$

where $\hat{c}^{\dagger}_{i,s}$ ($\hat{c}_{i,s}$) creates (annihilates) an electron on site $i = (x_i, y_i)$ with spin species s and $\hat{S}_i = 1/2 \times \hat{c}^{\dagger}_{i,s} \hat{\sigma} \hat{c}_{i,s'}$ (herein $\hat{\sigma}$ is the Pauli matrix). The doubly occupied states are explicitly excluded in the Hilbert space. We consider electron hopping terms up to next-nearest neighbors (t') and set the nearest neighboring hopping t as the energy unit. We choose $J = 1/3$ which is relevant to cuprates. We intend to study the physics related to the electron doped cuprates in this work. But in principle, only hole doping is allowed in the t–t'–J model because double occupancy is excluded in the local Hilbert space. However, by connecting the t–t'–J model as the large U limit of the t'-Hubbard model and through a particle–hole transformation, we can investigate the electron doped cuprates by studying the hole doped t–t'–J model with the sign of t' reversed from -0.2 in cuprates to 0.2.[16,17] So in this work we study the model in Eq. (1) with $t = 1$, $t' = 0.2$ and $J = 1/3$. We study cylinders with size $L_x \times L_y$ (see Fig. 1) and impose periodic or anti-periodic boundary conditions (PBC or APBC) along the circumferential direction. We also apply an antiferromagnetic pinning field $h_{\rm m} \times \hat{S}_z$ with strength $h_{\rm m} = 0.5$ on the left open edges in the Hamiltonian in Eq. (1), which allows us to calculate spin density instead of the more demanding correlation function, and makes the DMRG calculation easier to converge. By carefully comparing DMRG results with and without pinning fields, we find magnetic pinning fields on the left edge have negligible effect in the bulk of the system (see Appendix A1 for detailed results). The average hole concentration away from half-filling is defined as $\delta = N_{\rm h}/N$ with $N_{\rm h} = \sum_i (1 - n_i)$ (herein $\hat{n}_i = \sum_s \hat{c}^{\dagger}_{i,s} \hat{c}_{i,s}$ and $N = L_x \times L_y$). We study dopings with $\delta = 1/12$, $1/8$ and $1/6$, which represent the most interesting region in the phase diagram of cuprates.

The method we employ in this work is DMRG, which can provide accurate results for ladder systems. In the calculations, the total particle number of each spin species and total S_z are conserved. For width-4 and width-6 systems, we push the number of the kept states to ensure the calculation is converged (with truncation error in the order of 10^{-6} for width-4 systems) or in the converged region (with truncation error in the order of 10^{-5} for width-6 systems). For width-8 systems,

within the kept states ($m = 30000$) that we can reach, the results depend on the starting state in the DMRG sweep. So we try different states (Neel and stripe) to start the DMRG calculation and try to determine which one is stable during the sweep.

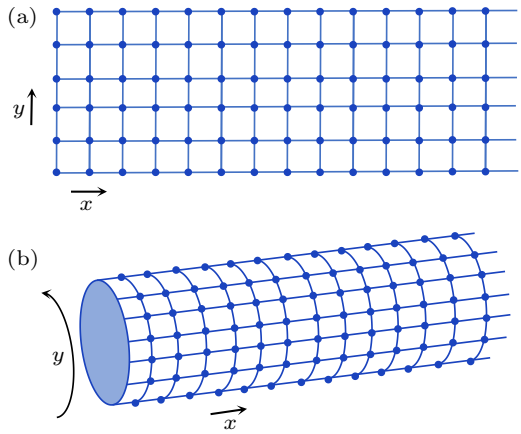


Fig. 1. (a) Square lattice adopted in the calculations and (b) the cylinder geometry. Periodic or anti-periodic boundary conditions are imposed along the circumferential direction.

3. Results

In Table 1, we summarize the results for spin and charge density as well as pair–pair correlation for the t–t'–J model on cylinders with different boundary conditions and widths for $1/12$, $1/8$ and $1/6$ dopings. For the pair–pair correlation, K_{sc} (ξ_{sc}) implies the system has a long-distance power (exponential)-law decaying behavior. The values of K_{sc} and ξ_{sc} are obtained from the fit of real-space pair–pair correlation functions with the reference bond set as the 8th vertical bond from the left edge, while the values in the parentheses are results by setting the reference bond as the 4th vertical bond from the left edge. In Table 1, we can find that the ground state switches between stripe and antiferromagnetic Neel states under different boundary conditions and widths. For all dopings, the pair–pair correlations are enhanced when the cylinder becomes wider from 4 to 6. The DMRG calculations for width 8 systems are not well converged for the largest kept states we can reach ($m = 30000$). But we try different starting states in the DMRG calculation and find that only Neel (stripe) state can be stabilized in DMRG calculation for $1/12$ ($1/6$) doping, while both stripe and Neel states are stable in the DMRG sweep for $1/8$ doping, regardless of the boundary conditions. These results indicate that $1/8$ doping is likely to lie on the boundary of the phase transition between the Neel and stripe phases, consistent with the previous study.[27] In the following, we discuss the details of the results.

Table 1. Summary of all the results, including the spin and charge densities, as well as the singlet pair–pair correlations. All systems have d-wave pairing symmetry except the $1/6$ doping case on width-4 cylinder under PBC, for which the pairing symmetry is plaquette d-wave.[23] K_{sc} and ξ_{sc} are obtained from the fit of pair–pair correlation with the reference bond set at the 8th (4th for the values in the parentheses) vertical bond from the left edge.

		Width-4		Width-6		Width-8	
		PBC	APBC	PBC	APBC	PBC	APBC
$1/12$	spin	Neel, short-ranged	filled stripe	Neel, short-ranged	Neel, (quasi) long-ranged	only Neel stablized	
	charge	half-filled stripe	filled stripe	1/3 filled stripe	1/3 filled stripe		
	pair	power-law, $K_{sc} \approx 1.1$ (0.98)	exponential, $\xi_{sc} \approx 9.82$ (9.9)	power-law, $K_{sc} \approx 0.49$ (0.49)	power-law, $K_{sc} \approx 0.48$ (0.41)		
$1/8$	spin	Neel, short-ranged	filled stripe	filled stripe, short-ranged	Neel, (quasi) long-ranged	both filled stripe & Neel stablized	
	charge	half-filled stripe	filled stripe	filled stripe, short-ranged	uniform		
	pair	power-law, $K_{sc} \approx 1.3$ (1.38)	exponential, $\xi_{sc} \approx 13.3$ (13.4)	power-law, $K_{sc} \approx 0.60$ (0.82)	power-law, $K_{sc} \approx 0.59$ (0.69)		
$1/6$	spin	stripe, short-ranged	filled stripe	filled stripe, short-ranged	Neel,(quasi) long-ranged	only filled stripe stablized	
	charge	modulated stripe	filled stripe	filled stripe, short-ranged	uniform		
	pair	power-law, $K_{sc} \approx 1.5$ (1.8)	exponential, $\xi_{sc} \approx 14.4$ (14.3)	power-law, $K_{sc} \approx 1.0$ (1.2)	power-law, $K_{sc} \approx 0.76$ (0.83)		

3.1. Spin and charge densities

We firstly discuss spin and charge properties. The staggered spin density is defined as $(-1)^{i_x+i_y} \times \langle \hat{S}_i^z \rangle$ with $\hat{S}_i^z = 1/2 \times (n_{i\uparrow} - n_{i\downarrow})$ and the charge density is defined as the average density along the circumference direction $n_i = \sum_{y=1}^{L_y} \langle n(i_x, i_y) \rangle / L_y$.

3.1.1. Width-4 results

Figure 2 displays the staggered spin density and electron density for doping levels of $1/12$ (upper panel), $1/8$ (middle panel) and $1/6$ (lower panel) on width-4 cylinders under PBC (left two columns) and APBC (right two columns). Results for different kept states in DMRG calculations are plotted and we can find good convergence of the results with kept states.

We start with results under PBC. For $1/12$ and $1/8$ dopings, the staggered spin density has the same sign and decays exponentially (see the insets of Figs. 2(a) and 2(e)) with the distance to the antiferromagnetic pinning fields on the left open edge, indicating the systems have short-ranged Neel correlation, while the charge density shows a half-filled

stripe structure with periodic amplitude modulation with wavelength $\lambda = 1/(2\delta)$. When the doping level increases to $1/6$, the spin density displays short-ranged stripe structure and the charge density has small fluctuations without a clear pattern.

The ground states, however, exhibit distinct characteristics under APBC as shown in the right two columns of Fig. 2. For all the three dopings, we find that the staggered spin density displays a spatial modulation with a wavelength ($\lambda = 2/\delta$) twice that of the charge density and has a π phase flip at the hole-concentrated sites, indicating the systems all have a filled stripe ground state.

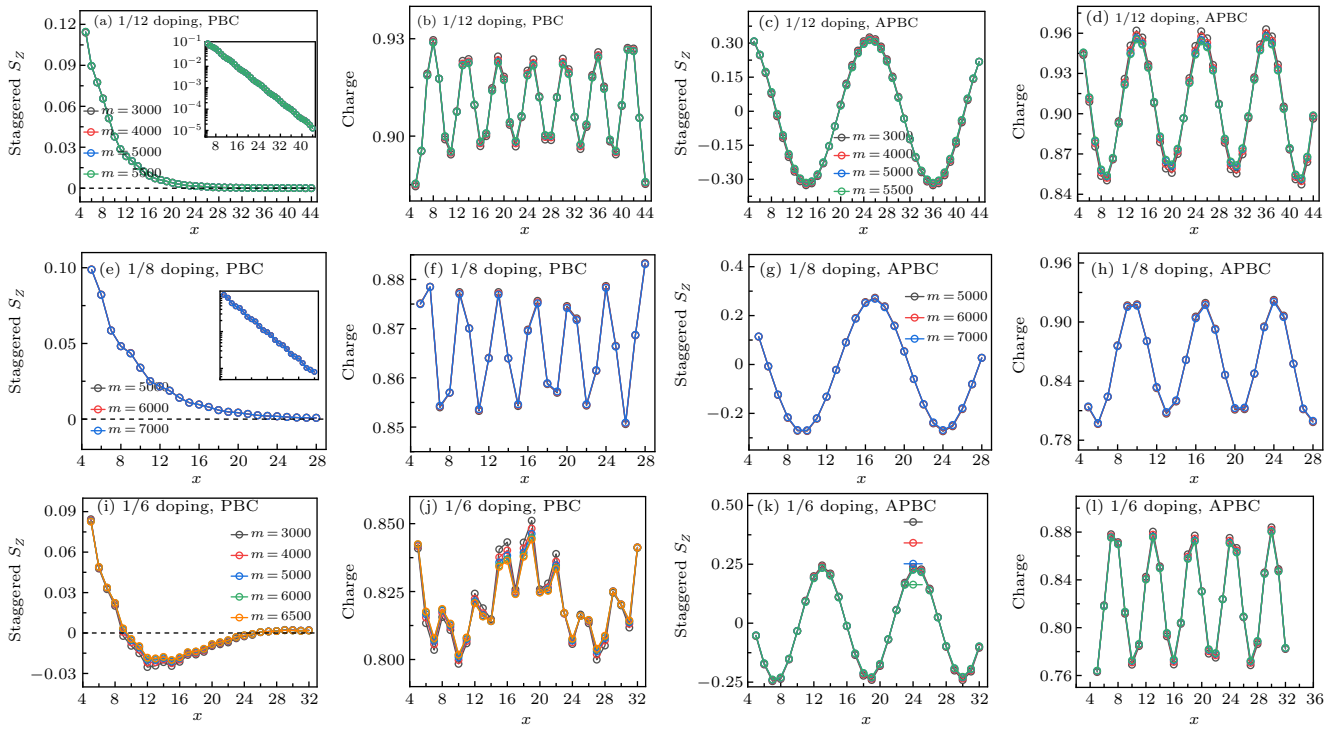


Fig. 2. Staggered spin density and electron density for $1/12$ (upper panel), $1/8$ (middle panel) and $1/6$ (lower panel) dopings on width-4 cylinders (system sizes are 4×48, 4×32 and 4×36 for $1/12$, $1/8$ and $1/6$ dopings, respectively) under PBC (left two columns) and APBC (right two columns). Results of finite kept states are plotted to show the convergence of the DMRG calculations. The insets in panels (a) and (e) are plotted in semi-logarithmic scale to show the exponential decay of the staggered spin density for $1/12$ and $1/8$ dopings under PBC. The dashed horizontal lines represent zero for the staggered spin density.

3.1.2. Width-6 results

As demonstrated above, the sensitivity of ground state to boundary conditions in width-4 system reflects the nonnegligible finite size effect in the model, so we extend our investigation into width-6 systems. We show the staggered spin density and electron density for $1/12$ (upper panel), $1/8$ (middle panel) and $1/6$ (lower panel) dopings on width-6 cylinders under PBC (left two columns) and APBC (right two columns) in Fig. 3. We also present results with different kept states to illustrate the convergence process during DMRG calculations.

For $1/12$ doping under both PBC and APBC on the upper panel of Fig. 3, we find that the spin density is Neel-type (no sign change in staggered spin density) and charge has $1/3$ filled stripe structure (with wavelength $\lambda = 1/(3\delta)$), though the Neel order in spin density is short-ranged (see exponentially-decaying behaviors in the inset of Fig. 3(a)) under PBC but (quasi) long-ranged under APBC.

The staggered spin and charge density profiles for both $1/8$ and $1/6$ dopings are shown on the remaining panels of Fig. 3. Spin and charge densities display short-range filled stripe order under PBC, but they have quasi-long-range Neel order in spin density with nearly uniform charge density under APBC.

Delving deeper into the spin structures of the model, the antiferromagnetic Neel correlation in the spin density at $1/12$ doping level appears to be firmly established on the width-6 cylinders. However, for doping levels of $1/8$ and $1/6$, the nature of the ground state varies with different boundary conditions applied. Additionally, it is observed that the ground states differ between width-4 and width-6 systems, even when subjected to the same doping and boundary conditions. This observation underscores the significant impact of finite size effects in the model.

3.1.3. Width-8 results

As anticipated, the DMRG calculations for width-8 systems is still a formidable challenge due to the linear increase in entanglement entropy with the cylinder's width. Even with the maximum kept states we can achieve ($m = 30000$ in the $U(1) \times U(1)$ symmetry sector), the truncation error in the DMRG calculations remains at the order of 10^{-4}, indicat-

ing that the calculations have not yet reached a satisfactory level of convergence. To overcome this problem, we proceed with DMRG calculations initiated from various starting states, including antiferromagnetic Neel and filled stripe configurations, in an effort to ascertain their stability throughout the DMRG sweep process. We find that for width-8 system, only Neel (stripe) state can be stabilized in DMRG calculation for $1/12$ ($1/6$) doping, while both stripe and Neel states are stable in the DMRG sweep for $1/8$ doping, regardless of the boundary conditions. The stable states are depicted in Fig. 4 for the $1/12$ and $1/6$ dopings, and in Fig. 5 for the $1/8$ doping scenario. We notice that the Neel state at $1/12$ doping persists in the width-8 system from the width-6 system and the charge is more uniform in the width-8 system. Besides, both filled stripe and Neel states are stable at $1/8$ doping on width-8 cylinders but exhibit a switching behavior on width-6 cylinders under different boundary conditions, consistent with the previous study.[27] The fact that both filled stripe and Neel states are stable in the DMRG sweep for $1/8$ doping suggests that $1/8$ doping level may reside at the cusp of a phase transition, marking the boundary between the Neel state at lower doping levels and the stripe state at higher ones.

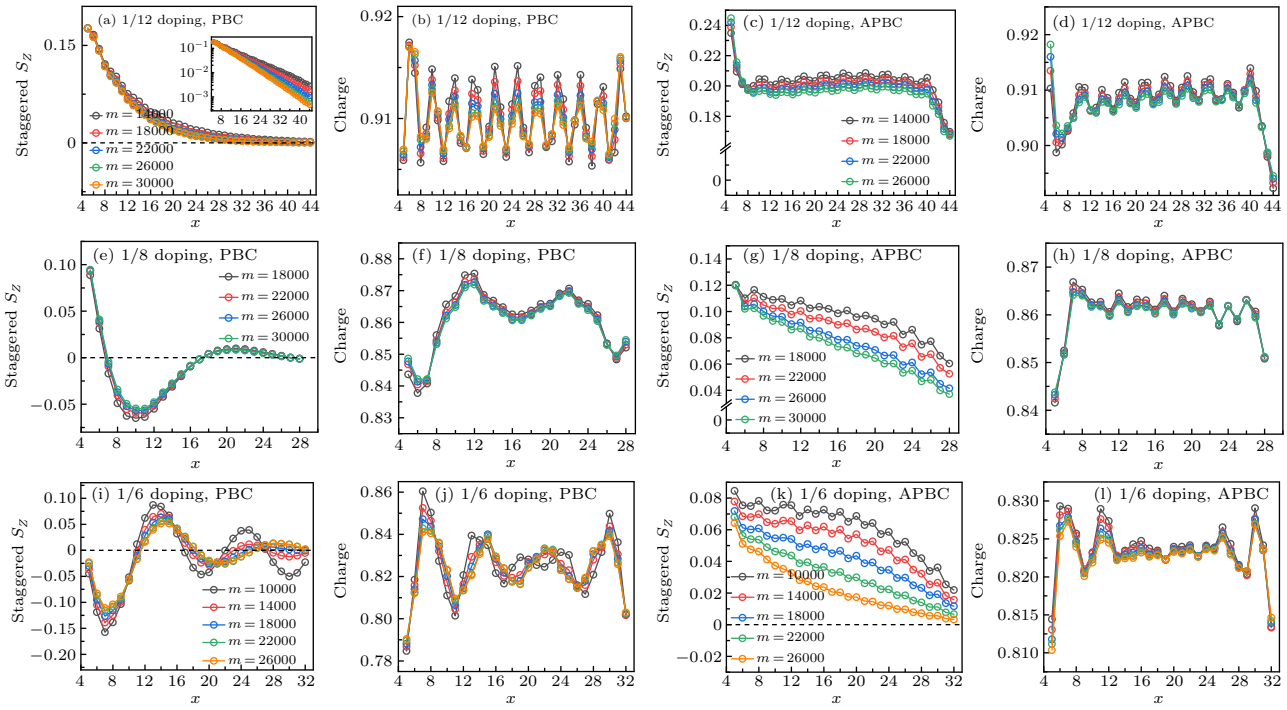


Fig. 3. Similar to Fig. 2 but for systems with width 6. Staggered spin density and electron density for $1/12$ (upper panel), $1/8$ (middle panel) and $1/6$ (lower panel) dopings on width-6 cylinders (system sizes are 6×48, 6×32 and 6×36 for $1/12$, $1/8$ and $1/6$ dopings, respectively) under PBC (left two columns) and APBC (right two columns). Results of finite kept states are plotted to show the convergence of the DMRG calculations. The inset in panel (a) is plotted in semi-logarithmic scale to show the exponential decay of the staggered spin density for $1/12$ doping under PBC. The dashed horizontal lines represent zero for the staggered spin density.

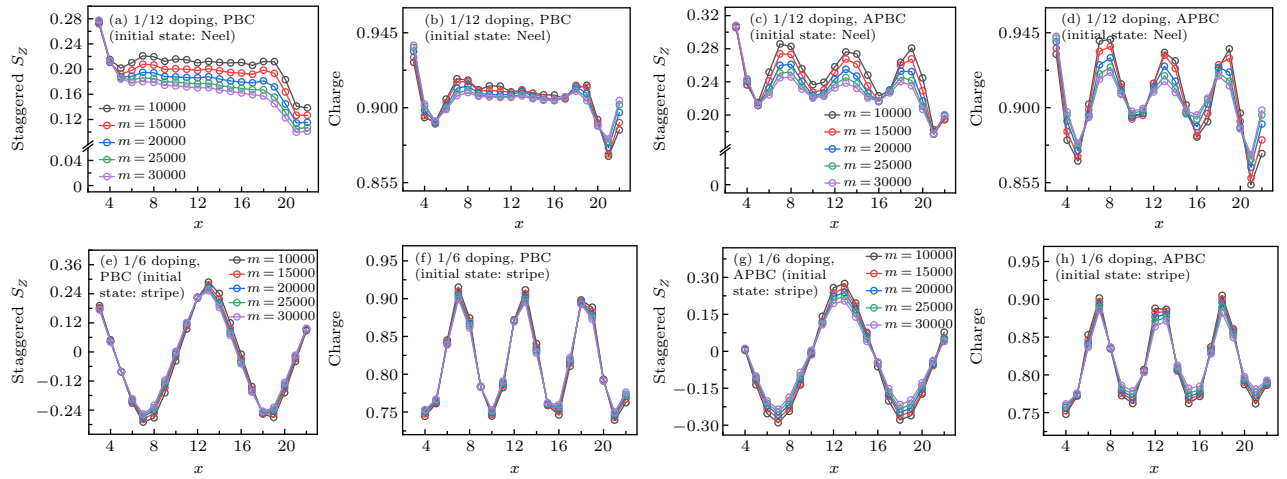


Fig. 4. Staggered spin density and electron density for $1/12$ (upper panel)and $1/6$ (lower panel) dopings (system sizes for both dopings are 8×24) on width-8 cylinders with PBC (left two columns) and APBC (right two columns). We try both Neel and filled stripe states as the starting states in the DMRG calculations but only Neel (stripe) state can be stabilized in the DMRG sweeps for $1/12$ ($1/6$) doping. We only show the numerically stabilized states.

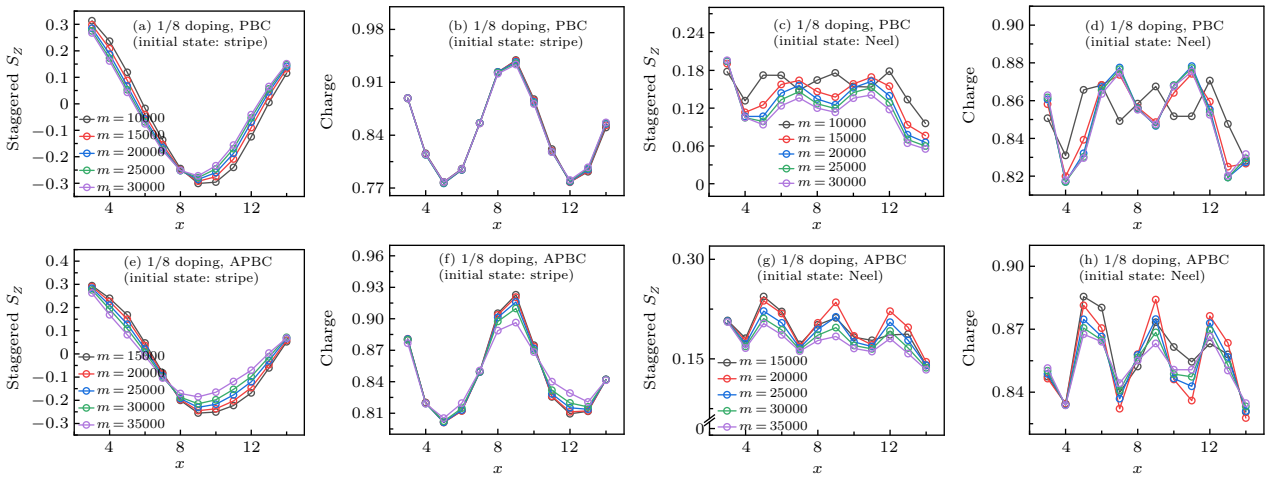


Fig. 5. Staggered spin density and electron density for $1/8$ doping levels on width-8 cylinders (8×16) with PBC (upper panel) and APBC (lower panel). In the DMRG sweep, both Neel and filled stripe states can be stabilized.

It is interesting to relate our findings to cuprates. On the electron-doped side of the phase diagram for cuprates, the antiferromagnetic Neel phase in the undoped parent compounds extends to electron doping levels exceeding 0.1. In our calculations, while a precise extrapolation with system width is not feasible, it is highly likely that the ground state for $1/12$ doping has antiferromagnetic Neel order. In this sense, the t–t'–J model is in accordance with cuprates.

3.2. Pairing correlation

The singlet pair–pair correlation function between bond i (the reference bond, consisting of sites (i_x, i_y) and $(i_x, i_y + 1)$) and bond $i + r$, defined as $D(r) = \langle \hat{\Delta}_i^\dagger \hat{\Delta}_{i+r} \rangle$ with $\hat{\Delta}_i^\dagger = 1/\sqrt{2}(\hat{c}^\dagger_{(i_x,i_y),\uparrow}\hat{c}^\dagger_{(i_x,i_y+1),\downarrow} - \hat{c}^\dagger_{(i_x,i_y),\downarrow}\hat{c}^\dagger_{(i_x,i_y+1),\uparrow})$, is shown in Fig. 6 for width-4 cylinders and Fig. 7 for width-6 cylinders. The pairing symmetry is found to be d-wave with opposite signs for vertical and horizontal bonds except the width-4 PBC system at $1/6$ doping, for which the pairing symmetry is plaquette d-wave.[23] As mentioned above, the width-8 calculations are not well converged, thus we do not show the pair–pair correlation for width-8 systems. In Figs. 6 and 7, both results for finite kept states and the extrapolated results with truncation error are shown.

We only show representative results for $D(r)$ with reference bond as the 8th vertical bond (consisting of site (8, 2) and site (8, 3)) from the left open edge. It is known that the value of $D(r)$ depends on the position of reference bond.[44] We also calculate $D(r)$ with reference bond as the 4th vertical bond (consisting of site (4, 2) and site (4, 3)). The results don't change qualitatively but there are indeed variations in the correlation lengths/exponents (see Table 1).

3.2.1. Width-4 results

Figure 6 shows the pair–pair correlation function $D(r)$ for width-4 systems. The numerical results are carefully extrapolated with truncation errors to remove the finite kept state effect. We find that for all dopings, $D(r)$ decays algebraically with exponent K_{sc} as $D(r) \propto r^{-K_{sc}}$ (exponentially with correlation length ξ_{sc} as $D(r) \propto e^{-r/\xi_{sc}}$) under PBC (APBC) in a modulated manner with the period of charge density wavelength. The difference in ground state between systems under PBC and APBC is also observed for spin and charge densities in Fig. 2. The fitted exponents K_{sc} or correlation length ξ_{sc} using the extrapolated data are also shown in Fig. 6. We notice that for the system under APBC, when the spin and charge

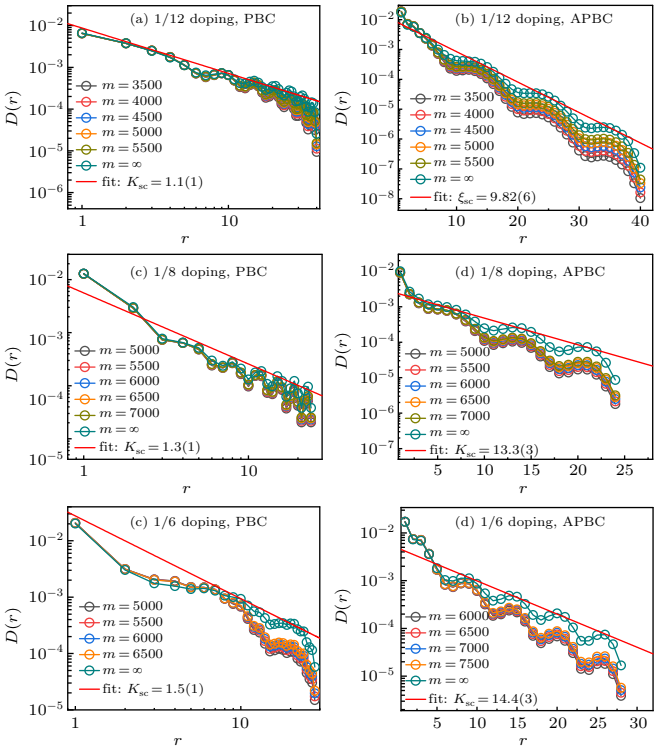


Fig. 6. Singlet pair–pair correlation for $1/12$ (upper panel), $1/8$ (middle panel) and $1/6$ (lower panel) dopings on width-4 cylinders under PBC (left) and APBC (right). The reference bond is placed at the bond consisting of sites (8, 2) and (8, 3). Both results for finite kept states and the extrapolated results with truncation error are shown. Solid lines are algebraic (left) and exponential (right) fits of extrapolated data. Only peaked values are used in the fits for the pair–pair correlation function. The correlation lengths or exponents are listed in the legend.

density show a strong filled stripe state, $D(r)$ decays exponentially. This relationship indicates that a strong filled stripe state is harmful for pairing as seen in the pure Hubbard model.[15]

3.2.2. Width-6 results

Figure 7 shows the pair–pair correlation function $D(r)$ for width-6 systems. For all the results in Fig. 7, $D(r)$ has a fast decaying tail which bends upward with the increase of kept states. We attribute this tail to the intrinsic consequence of finite number of kept states in DMRG calculations since the matrix-product state always exhibits exponentially decaying correlations at long distances[45] when the bond dimension is not large enough. From the data we find the extrapolation of $D(r)$ with truncation error at the tail is not as reliable as at the head. We also notice that the behavior of $D(r)$ for $r \leq 4$ does not fit in the long-range behavior. These observations are also consistent with the BCS analysis that pair–pair correlation $D(r)$ at intermediate distances already equals to those of the two-dimensional system.[46] Thus the small r and very large r data are not included when performing the fit of $D(r)$ to obtain the exponent K_{sc}.

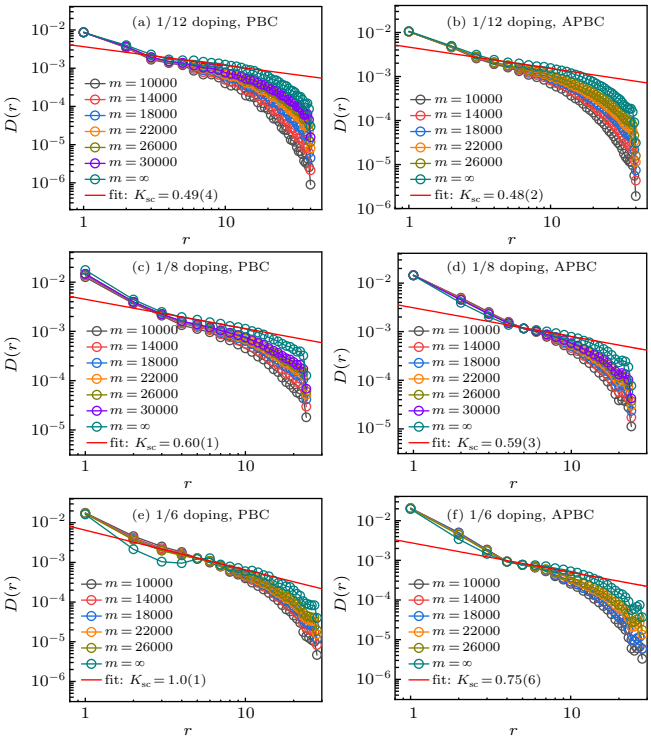


Fig. 7. Similar to Fig. 6 but for width 6 cylinders. Singlet pair–pair correlation for $1/12$ (upper panel), $1/8$ (middle panel) and $1/6$ (lower panel) dopings on width-6 cylinders with PBC (left) and APBC (right). The reference bond is placed at the bond consisting of sites (8, 2) and (8, 3). Both results for finite kept states and extrapolated results with truncation error are shown. Solid lines are algebraic fits of the extrapolated data and the corresponding exponents are listed in the legend.

For all doping and boundary conditions, $D(r)$ decays polynomially for width-6 systems as shown in Fig. 7. Since the static pair–pair superconducting susceptibility diverges as $\chi_{sc}(T) = T^{-(2-K_{sc})}$, all the systems display quasi long-range pairing with $K_{sc} < 2$ as T approaches 0 K. For fixed doping, the difference of K_{sc} between systems under PBC and APBC is small. Moreover, for all the dopings, K_{sc} is reduced compared to the width-4 results in Fig. 6. Similar conclusion can be found in works such as Ref. [29]. The coexistence of 1/3 charge stripe and d-wave superconductivity at $1/12$ doping but a robust superconducting phase with short-ranged spin and charge order at 1/8 and 1/6 dopings under PBC is consistent with results from Ref. [25]. We also notice the increase of K_{sc} when the doping is reduced.

4. Discussion

It was known that the filled stripe state is stable in the pure Hubbard model for different widths,[15] where long-range pairing is notably absent. In the t–t'–J model, we also notice that when strong filled stripe order is found in the ground state for the width-4 system under APBC, superconducting pairing is also short-ranged. This correlation suggests that a robust filled stripe order may potentially impede the emergence of superconductivity. In other cases, short-range stripe states with fractional fillings are accompanied with quasi-long-ranged superconducting pairing. In general, the t' term makes the electron more mobile, causing the paired electrons in the stripe state[15] to gain coherence and consequently, exhibit superconductivity.[40] The pronounced sensitivity of the ground state in both the t–t'–J and t'-Hubbard models[40] to boundary conditions and system widths can be interpreted as an indication of the stripe state's vulnerability when the t' term is incorporated. These findings underscore the critical importance of scrutinizing finite size effects in forthcoming research on systems confined to narrow cylinders, ensuring a comprehensive understanding of the interplay between stripe order and superconductivity.

5. Conclusion and perspective

We study the finite size effect in the electron doped t–t'–J model on cylinders. We have identified the notable sensitivity of the ground state to both boundary conditions and system width, congruent with previous findings in the t'-Hubbard model.[40] For width-4 and width-6 systems, the ground state switches between Neel and stripe states under different boundary conditions and different system widths. For the width-8 system and up to the number of kept states we can reach, only Neel (stripe) state can be stabilized in DMRG calculation for $1/12$ ($1/6$) doping, while both stripe and Neel states are stable in the DMRG sweep for $1/8$ doping, regardless of the boundary conditions. These results indicate that $1/8$ doping is likely to lie in the boundary of the phase transition between the Neel phase at lower doping and the stripe phase at higher doping, consistent with previous studies.[27] Our results offer

useful insights into the ground state of the electron doped t–t'–J model by adopting the boundary condition and system size as useful indicators and underscore the necessity of checking the finite size and boundary condition effect in the future study of systems on narrow cylinders. It will be interesting to also analyze the finite size effect in the hole doped region in the future, which is more complicated due to different competing states in the ground state.[9]

Appendix A

A1. Effect of magnetic pinning fields

To evaluate the effect of the pinning fields, we carefully compare the results from DMRG calculations with and without pinning fields for the 1/8 doping case. Figure A1 shows the charge and spin density (correlation) on the width-4 (4×32) cylinders under periodic and anti-periodic boundary conditions. Here we only present converged results with truncation error $\sim 10^{-7}$. We find the charge density exhibits the similar behavior with the same wavelength with and without the pinning fields, indicating pinning fields at the left edge have tiny impact on the charge density only for sites near the boundary. Without magnetic pinning fields, we can only calculate spin-spin correlation to probe the magnetic structure. We find the magnetic structures are the same with and without pinning fields. We find the value of spin-spin correlation is much smaller than local spin density, so it is better to probe the magnetic correlation in a system by applying pinning fields at the edges.

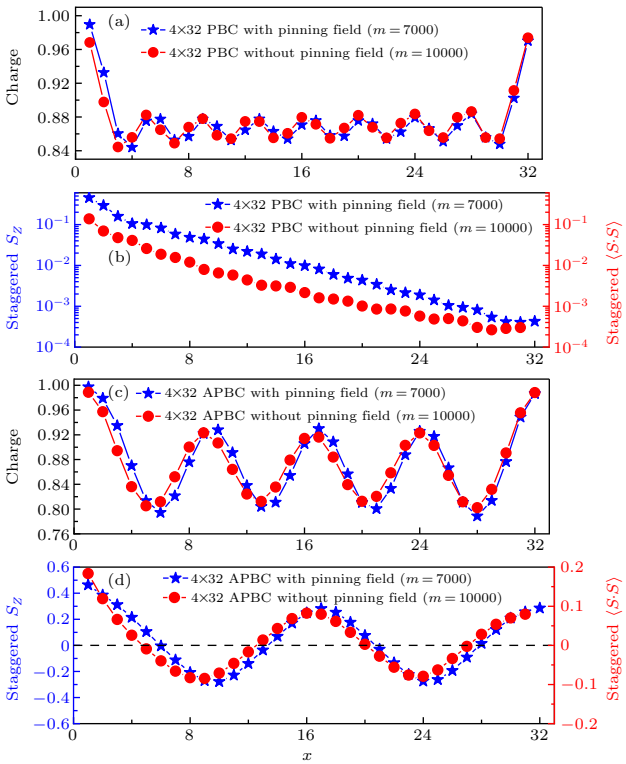


Fig. A1. Charge and spin densities (correlation) on 4×32 cylinders under PBC (a), (b) and APBC (c), (d) with and without magnetic pinning fields for the 1/8 doping case. The results show that the edge pinning fields have tiny effect on the bulk properties of the system.

A2. Larger-length results for width-4 systems

We show a comparison of DMRG results for 4×32 and 4×64 systems under PBC and APBC at 1/8 doping in Fig. A2. We only show converged results with truncation error in the order of 10^{-6}. We can find systems with different length have the same charge and spin distributions. These results imply that the system with length 32 is already long enough to study the spin and charge structures in the model.

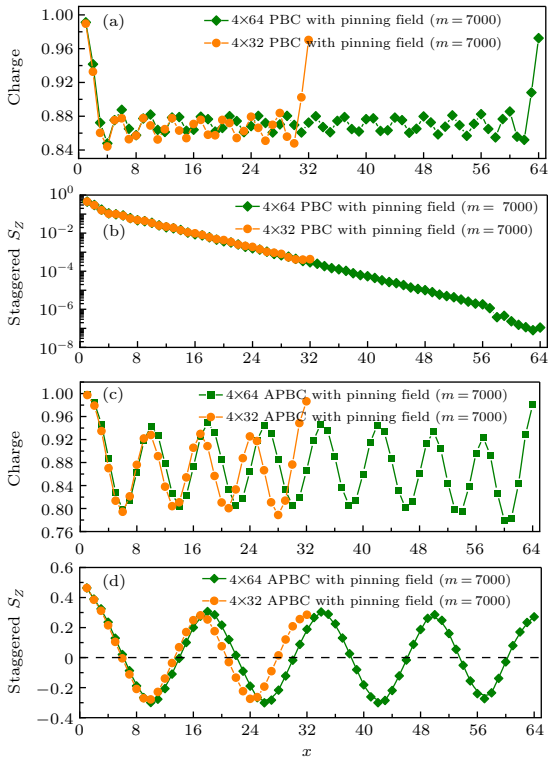


Fig. A2. Comparison of charge and spin densities on 4×32 and 4×64 cylinders under PBC (a), (b) and APBC (c), (d) with magnetic pinning fields on the left edge for the 1/8 doping case. The wavelength and decaying behaviors are the same for the two systems, indicating a system with length 32 is long enough for the study of the model.

Acknowledgments

We thank Shiwei Zhang, Steven R. White, Ulrich Schollwöck, Hao Xu, and Chia-Min Chung for useful discussions. We thank Kang Wang for useful suggestions on the manuscript. The calculation in this work is carried out with TensorKit.[47] The computation in this paper were run on the Siyuan-1 cluster supported by the Center for High Performance Computing at Shanghai Jiao Tong University. Shen and Qin thank Weidong Luo for his generosity to provide computational resources.

Project supported by the National Key Research and Development Program of China (Grant No. 2022YFA1405400), the Innovation Program for Quantum Science and Technology

(Grant No. 2021ZD0301902), the National Natural Science Foundation of China (Grant No. 12274290), and the sponsorship from Yangyang Development Fund.

References

[1] Hubbard J 1963 *Proc. R. Soc. Lond. Ser. A* **276** 238
[2] Zhang F C and Rice T M 1988 *Phys. Rev. B* **37** 3759
[3] Qin M, Schäfer T, Andergassen S, Corboz P and Gull E 2022 *Annu. Rev. Condens. Matter Phys.* **13** 275
[4] Arovas D P, Berg E, Kivelson S A and Raghu S 2022 *Annu. Rev. Condens. Matter Phys.* **13** 239
[5] LeBlanc J P F, Antipov A E, Becca F, Bulik I W, Chan G K L, Chung C M, Deng Y, Ferrero M, Henderson T M, Jiménez-Hoyos C A, Kozik E, Liu X W, Millis A J, Prokofév N V, Qin M, Scuseria G E, Shi H, Svistunov B V, Tocchio L F, Tupitsyn I S, White S R, Zhang S, Zheng B X, Zhu Z and Gull E 2015 *Phys. Rev. X* **5** 041041
[6] Corboz P, Rice T M and Troyer M 2014 *Phys. Rev. Lett.* **113** 046402
[7] Corboz P, White S R, Vidal G and Troyer M 2011 *Phys. Rev. B* **84** 041108
[8] Chou C P and Lee T K 2010 *Phys. Rev. B* **81** 060503
[9] Scalapino D J 2012 *Rev. Mod. Phys.* **84** 1383
[10] Dagotto E 1994 *Rev. Mod. Phys.* **66** 763
[11] Anderson P W 1987 *Science* **235** 1196
[12] Keimer B, Kivelson S A, Norman M R, Uchida S and Zaanen J 2015 *Nature* **518** 179
[13] Zheng B X, Chung C M, Corboz P, Ehlers G, Qin M P, Noack R M, Shi H, White S R, Zhang S and Chan G K L 2017 *Science* **358** 1155
[14] Xu H, Shi H, Vitali E, Qin M and Zhang S 2022 *Phys. Rev. Res.* **4** 013239
[15] Qin M, Chung C M, Shi H, Vitali E, Hubig C, Schollwöck U, White S R and Zhang S 2020 *Phys. Rev. X* **10** 031016
[16] Andersen O, Liechtenstein A, Jepsen O and Paulsen F 1995 *J. Phys. Chem. Solids* **56** 1573
[17] Hirayama M, Yamaji Y, Misawa T and Imada M 2018 *Phys. Rev. B* **98** 134501
[18] White S R and Scalapino D J 1999 *Phys. Rev. B* **60** R753
[19] Martins G B, Xavier J C, Gazza C, Vojta M and Dagotto E 2000 *Phys. Rev. B* **63** 014414
[20] Martins G B, Xavier J C, Arrachea L and Dagotto E 2001 *Phys. Rev. B* **64** 180513
[21] Jiang Y F, Zaanen J, Devereaux T P and Jiang H C 2020 *Phys. Rev. Res.* **2** 033073
[22] Dodaro J F, Jiang H C and Kivelson S A 2017 *Phys. Rev. B* **95** 155116
[23] Chung C M, Qin M, Zhang S, Schollwöck U and White S R 2020 *Phys. Rev. B* **102** 041106
[24] Huang E W, Mendl C B, Jiang H C, Moritz B and Devereaux T P 2018 *npj Quantum Mater.* **3** 22
[25] Gong S, Zhu W and Sheng D N 2021 *Phys. Rev. Lett.* **127** 097003
[26] Jiang H C and Kivelson S A 2021 *Phys. Rev. Lett.* **127** 097002
[27] Jiang S, Scalapino D J and White S R 2021 *Proc. Natl. Acad. Sci. USA* **118** e2109978118
[28] Lu X, Zhang J X, Gong S S, Sheng D and Weng Z Y 2024 *Phys. Rev. B* **110** 165127
[29] Lu X, Chen F, Zhu W, Sheng D N and Gong S S 2024 *Phys. Rev. Lett.* **132** 066002
[30] Jiang S, Scalapino D J and White S R 2022 *Phys. Rev. B* **106** 174507
[31] Marino V, Becca F and Tocchio L F 2022 *SciPost Phys.* **12** 180
[32] Ponsioen B, Chung S S and Corboz P 2019 *Phys. Rev. B* **100** 195141
[33] Chen Q, Qiao L, Zhang F and Zhu Z 2019 *Phys. Rev. B* **110** 045134
[34] Chen F, Haldane F D M and Sheng D N 2019 *Proc. Natl. Acad. Sci. USA* **122** e2420963122
[35] Jiang H C and Devereaux T P 2019 *Science* **365** 1424
[36] White S R and Scalapino D J 2009 *Phys. Rev. B* **79** 220504
[37] Tohyama T and Maekawa S 1994 *Phys. Rev. B* **49** 3596
[38] Tohyama T 2004 *Phys. Rev. B* **70** 174517
[39] Himeda A, Kato T and Ogata M 2002 *Phys. Rev. Lett.* **88** 117001
[40] Xu H, Chung C M, Qin M, Schollwöck U, White S R and Zhang S 2024 *Science* **384** eadh7691
[41] White S R 1992 *Phys. Rev. Lett.* **69** 2863
[42] White S R 1993 *Phys. Rev. B* **48** 10345
[43] Schollwöck U 2011 *Ann. Phys.* **326** 96
[44] Shen Y, Zhang G M and Qin M 2023 *Phys. Rev. B* **108** 165113
[45] Dolfi M, Bauer B, Keller S and Troyer M 2015 *Phys. Rev. B* **92** 195139
[46] Gannot Y and Kivelson S A 2023 *Phys. Rev. B* **107** 075127
[47] Our in-house DMRG code is developed with TensorKit package at https://github.com/Jutho/TensorKit.jl